Demystifying the growth of superconducting Sr_2RuO_4 thin films

Hari P. Nair, Jacob P. Ruf, Nathaniel J. Schreiber, et al.

View Online   Export Citation   CrossMark

ARTICLES YOU MAY BE INTERESTED IN

Synthesis science of $SrRuO_3$ and $CaRuO_3$ epitaxial films with high residual resistivity ratios
APL Materials **6**, 046101 (2018); https://doi.org/10.1063/1.5023477

Molecular beam epitaxy growth of superconducting Sr_2RuO_4 films
APL Materials **5**, 106108 (2017); https://doi.org/10.1063/1.5007342

Growth of superconducting Sr_2RuO_4 thin films
Applied Physics Letters **97**, 082502 (2010); https://doi.org/10.1063/1.3481363

APL Materials

SPECIAL TOPIC:
Materials Challenges for Supercapacitors

Submit Today!

Demystifying the growth of superconducting Sr$_2$RuO$_4$ thin films

Hari P. Nair,[1] Jacob P. Ruf,[2] Nathaniel J. Schreiber,[1] Ludi Miao,[2] Morgan L. Grandon,[1] David J. Baek,[3] Berit H. Goodge,[4,5] Jacob P. C. Ruff,[6] Lena F. Kourkoutis,[4,5] Kyle M. Shen,[2,5] and Darrell G. Schlom[1,5]

[1]*Department of Materials Science and Engineering, Cornell University, Ithaca, New York 14853, USA*
[2]*Department of Physics, Cornell University, Ithaca, New York 14853, USA*
[3]*School of Electrical and Computer Engineering, Cornell University, Ithaca, New York 14853, USA*
[4]*School of Applied and Engineering Physics, Cornell University, Ithaca, New York 14853, USA*
[5]*Kavli Institute at Cornell for Nanoscale Science, Ithaca, New York 14853, USA*
[6]*Cornell High Energy Synchrotron Source, Cornell University, Ithaca, New York 14853, USA*

We report the growth of superconducting Sr$_2$RuO$_4$ thin films by molecular-beam epitaxy on (110) NdGaO$_3$ substrates with transition temperatures of up to 1.8 K. We calculate and experimentally validate a thermodynamic growth window for the adsorption-controlled growth of superconducting Sr$_2$RuO$_4$ epitaxial thin films. The growth window for achieving superconducting Sr$_2$RuO$_4$ thin films is narrow in growth temperature, oxidant pressure, and ruthenium-to-strontium flux ratio. © *2018 Author(s). All article content, except where otherwise noted, is licensed under a Creative Commons Attribution (CC BY) license (http://creativecommons.org/licenses/by/4.0/).* https://doi.org/10.1063/1.5053084

With strong evidence of topologically non-trivial pairing symmetry (e.g., possibly $p_x \pm ip_y$),[1–9] Sr$_2$RuO$_4$ is a candidate for odd-parity superconductivity.[1,5,8] The superconducting transition temperature (T_c), defined as the midpoint (with respect to resistivity) of the superconducting transition,[10–12] of extremely pure Sr$_2$RuO$_4$ single crystals is 1.5 K.[11,13] Recently, it was demonstrated that uniaxial strain can significantly enhance the T_c of Sr$_2$RuO$_4$ single crystals from 1.5 K to 3.4 K.[14,15] This enhancement has been attributed to the Van Hove singularity moving closer to the Fermi level with strain. Direct measurement of the effect of epitaxial strain on the Fermi surface of Sr$_2$RuO$_4$ thin films using angle-resolved photoemission spectroscopy (ARPES) has revealed that the topology of the Fermi surface is very sensitive to epitaxial strain.[16] Due to the extreme sensitivity of the superconducting ground state in Sr$_2$RuO$_4$ to disorder,[12,17] lattice strain is the only viable method, to date, to tune the superconducting ground state of Sr$_2$RuO$_4$. This makes reproducible growth of superconducting Sr$_2$RuO$_4$ thin films important for enabling (1) epitaxial strain to be used to enhance T_c,[18] (2) epitaxial heterostructures to be grown to assess and establish the pairing symmetry of Sr$_2$RuO$_4$,[19–21] and (3) Sr$_2$RuO$_4$-based heterostructures to be scaled to large-area films to provide the practical foundation of a scalable ground-state quantum computing technology.[22,23]

Although extremely pure Sr$_2$RuO$_4$ single crystals have been synthesized, with residual resistivities less than 100 nΩ·cm,[13] there are very few reports of superconducting Sr$_2$RuO$_4$ thin films.[24–26] The T_cs of these films are lower than those of the best single crystals, likely due to a combination of planar[17,27–29] and point defects,[12] which can act as pair breakers.

In this letter, we outline and experimentally validate an adsorption-controlled growth window for realizing superconducting Sr$_2$RuO$_4$ thin films. Our approach not only reproducibly produces superconducting Sr$_2$RuO$_4$ thin films (we have grown tens of superconducting Sr$_2$RuO$_4$ films) but also yields Sr$_2$RuO$_4$ films with the highest T_c reported to date. We hope that describing this growth regime and rationale in detail will clarify some of the mysteries surrounding the growth of superconducting Sr$_2$RuO$_4$ thin films and spur further exploration of heterostructures involving superconducting Sr$_2$RuO$_4$ in thin film form.

In a previous publication,[30] we introduced the thermodynamics of molecular-beam epitaxy (TOMBE) diagram to discuss the adsorption-controlled growth of ruthenates. The TOMBE diagram is particularly helpful for visualizing the growth window of compounds where multiple volatile gas species are inherently involved in the growth. In the case of Sr_2RuO_4, like other complex oxide ruthenates, the gas species involved in calculating the growth window are $O_2(g)$ and $RuO_x(g)$ ($x = 2$ or 3).

The region shaded in red in the TOMBE diagram of the Sr-Ru-O ternary system (Fig. 1) illustrates the adsorption-controlled growth window of Sr_2RuO_4, where $Sr_2RuO_4(s)$ is in equilibrium with $RuO_x(g)$. The growth window in Fig. 1 has been calculated for an incident excess ruthenium flux of $1.3 \times 10^{13}/cm^2 \cdot s$, consistent with the growth conditions used in this manuscript. The growth window for phase-pure Sr_2RuO_4, shaded red region in Fig. 1, is rather narrow adding to the challenge for realizing superconducting Sr_2RuO_4 thin films. The growth window is narrow due to the small difference in Gibbs formation energies between $Sr_2RuO_4(s)$ and $Sr_3Ru_2O_7(s)$.[31] On the higher temperature and higher oxygen pressure side of the dotted red line, it is thermodynamically favorable for Sr_2RuO_4 to break down into $SrO(s)$ and $RuO_x(g)$, while on the lower temperature and lower oxygen pressure side of the dotted green line, the formation of $Sr_3Ru_2O_7(s)$ becomes thermodynamically favorable. Figure S1 of the supplementary material illustrates the effect of varying the excess ruthenium on the growth window with the incident ruthenium flux fixed at 2×10^{13} atoms/cm$^2 \cdot$s. As the excess ruthenium flux (determined by the ruthenium-to-strontium flux ratio) is reduced, the growth window for Sr_2RuO_4 expands.

The narrow growth window we calculate for Sr_2RuO_4 in Fig. 1 agrees with the observation of other groups that the growth window for superconducting Sr_2RuO_4 thin films is very narrow in terms of parameters such as the growth temperature[24] and ruthenium-to-strontium flux ratio.[26] This narrow growth window is the most significant challenge in reproducibly growing superconducting Sr_2RuO_4 thin films, requiring careful optimization of the interdependent growth parameters.

High substrate temperatures are critical for achieving superconducting Sr_2RuO_4 thin films; we attribute this to two underlying reasons. The first is that high substrate temperature enhances the adatom surface migration length, which increases the spacing between out-of-phase boundaries.[28] These out-of-phase boundaries propagate through the thickness of the film and can act as pair breakers, thus suppressing the fragile superconductivity in Sr_2RuO_4 thin films.[27] The second is that high
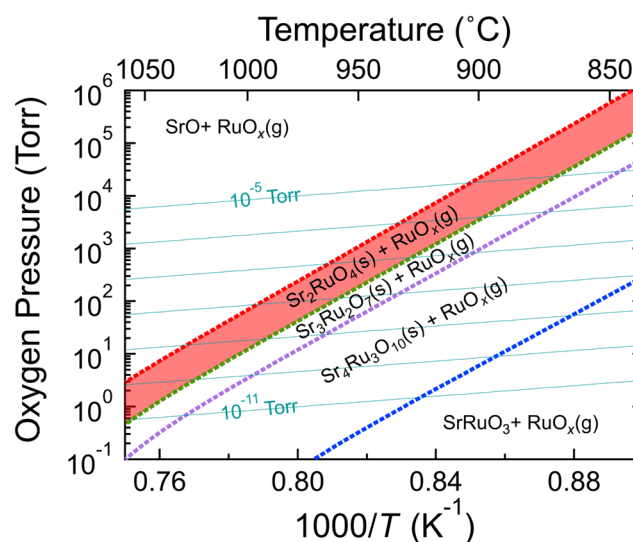
FIG. 1. TOMBE diagram for the $Sr_{n+1}Ru_nO_{3n+1}$ Ruddlesden Popper phases with the adsorption-controlled growth window for Sr_2RuO_4 highlighted in red. The cyan lines show the equivalent oxidation potential for ozone partial pressures ranging from 10^{-11}–10^{-5} Torr as explained in Ref. 30. The thermodynamic growth window for Sr_2RuO_4 is quite narrow underscoring the challenge in achieving superconducting Sr_2RuO_4 thin films.

substrate temperature is essential for overcoming any reaction kinetic bottlenecks and promotes growth within this thermodynamic window.[30]

   Sr_2RuO_4 thin films were grown using a Veeco GEN10 molecular-beam epitaxy system. Strontium was evaporated from a low-temperature effusion cell, while an electron beam evaporator was used for ruthenium. All of the elemental source materials had a purity of 99.99%. Distilled ozone (~80% O_3 + 20% O_2) was used as the oxidant, which was introduced into the chamber using a water-cooled, electropolished 316L stainless steel tube with a 4.6 mm inner diameter pointed at the substrate with an angle of inclination of 40° from the normal of the substrate and that terminates a distance of 9.6 cm from the center of the substrate. The tube provides an enhancement in the local oxidant pressure by a factor of ~4× over the background chamber pressure. An optical pyrometer operating at a wavelength of 1550 nm was used to measure the substrate temperature. (110) $NdGaO_3$ substrates, from CrysTec GmbH, were etched using $HF-NH_4OH$ and then annealed at 950 °C in flowing oxygen to yield a GaO_2-terminated surface.[32]

   The Sr_2RuO_4 thin film, characterized in detail in this manuscript, was grown on a (110) $NdGaO_3$ substrate within the adsorption-controlled growth window outlined in Fig. 1. We used a strontium flux of 2.2×10^{13} atoms/cm²·s and a ruthenium flux of 2.4×10^{13} atoms/cm²·s corresponding to an excess ruthenium flux of 1.3×10^{13} atoms/cm²·s for the growth of Sr_2RuO_4. The film was grown at a substrate temperature of 900 °C and a chamber background pressure of 8×10^{-7} Torr of (~80% O_3 + 20% O_2). At the end of the growth, both the strontium and ruthenium shutters were closed simultaneously and the sample was rapidly cooled to below 250 °C under the same ozone pressure as was used during growth. The growth conditions used here fall within the narrow growth window calculated in the TOMBE diagram in Fig. 1. This illustrates the accuracy of the calculations and confirms that our growth temperature is sufficiently high so that kinetic barriers are negligible and the growth can be accurately described by thermodynamics.

   X-ray diffraction (XRD) measurements along the specular crystal truncation rod (CTR) were carried out in a Rigaku SmartLab high-resolution diffractometer with Cu-$K_{\alpha 1}$ radiation (λ = 1.5406 Å). A Ge 220 double-crystal monochromator was used in the incident side optics for the XRD θ-2θ measurement. The XRD θ-2θ scan of a 55 nm thick Sr_2RuO_4 film grown on a (110) $NdGaO_3$ substrate (notations following the *Pbnm* non-standard setting of space group #62) is shown in Fig. 2. All of the peaks in the XRD θ-2θ scan can be indexed to either the (001)-oriented Sr_2RuO_4 film or the (110) $NdGaO_3$ substrate (asterisks). The out-of-plane lattice constant of the film is c = 12.772 ± 0.007 Å at room temperature, which is slightly larger than the room-temperature value of 12.746 Å for Sr_2RuO_4 single crystals,[33] consistent with the film being subject to a modest amount of in-plane compressive misfit strain imposed by the substrate. Specifically, the misfit strain in the Sr_2RuO_4 at room temperature on the (110) $NdGaO_3$ substrate[34] is −0.39% along the [001] in-plane direction of the substrate and −0.16% along the [1$\bar{1}$0] in-plane direction of the substrate. From an elastic stiffness calculation, $\epsilon_{33} = \frac{-c13}{c33}(\epsilon_{11} + \epsilon_{22})$, where ϵ_{11}, ϵ_{22}, and ϵ_{33} are the principal strains in the Sr_2RuO_4 film and c_{13} and c_{33} are the coefficients of the elastic stiffness tensor of Sr_2RuO_4 in Voigt notation,[35] this strain is expected to yield an out-of-plane film spacing 12.770 Å, which is in good agreement with the 12.772 ± 0.007 Å spacing observed. Rocking curve measurements around the 006 reflection of the Sr_2RuO_4 film and the 220 reflection of the $NdGaO_3$ substrate are shown in Fig. 2(b). In addition to the Ge 220 double-crystal monochromator on the incident side, a Ge 220 two-bounce analyzer was also used on the detector side to improve the resolution of the rocking curve measurements. The slits on the incident and receiving side optics were set to 1 mm. The full width at half maximum (FWHM) of the Sr_2RuO_4 film (20 arcsec) is comparable to the FWHM of the $NdGaO_3$ substrate (15 arcsec) indicating that the structural quality of the film is comparable to that of the underlying substrate.

   In addition to these lab-based XRD measurements, we also performed synchrotron-based non-resonant XRD measurements on other superconducting Sr_2RuO_4 films grown on (110) $NdGaO_3$ at beamline A2 at the Cornell High Energy Synchrotron Source (CHESS). Synchrotron data were taken using an incident energy of 14.5 keV (λ = 0.855 Å) and a Dectris Eiger X 1M area detector, to more thoroughly map the reciprocal space of these samples. A representative segment of an off-specular CTR with in-plane momentum transfer $q_{\parallel}$ along [001] $NdGaO_3$ is shown in Fig. 2(c) for a 132 nm thick Sr_2RuO_4 film grown on (110) $NdGaO_3$. The 107 reflection of Sr_2RuO_4 and the 222 reflection of
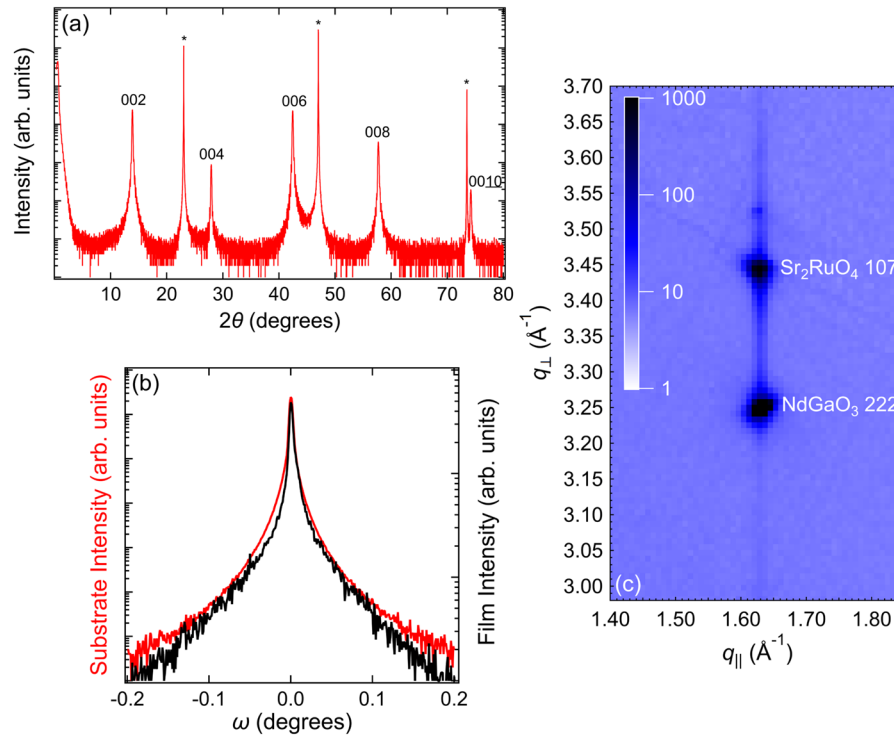
FIG. 2. (a) X-ray diffraction θ-2θ scan of a ~55 nm thick (001)-oriented Sr_2RuO_4 film grown on a (110) $NdGaO_3$ substrate. All of the peaks in the scan can be indexed to either the film or the substrate (asterisks). (b) Rocking curves in ω for the substrate (in red) and the film (in black). The rocking curve full width at half maximum for the Sr_2RuO_4 film is comparable to that of the (110) $NdGaO_3$ substrate; this is indicative of high structural quality. (c) Reciprocal space map of a 132 nm thick Sr_2RuO_4 film grown on a (110) $NdGaO_3$ substrate. The in-plane lattice constant of the film is the same as that of the substrate illustrating the absence of strain relaxation even for a 132 nm thick film. The $q_{\parallel}$ is along the [001] direction of the (110) $NdGaO_3$ substrate.

the (110) $NdGaO_3$ substrate are aligned with the same $q_{\parallel}$, showing that the in-plane lattice constants of the film and substrate are equal illustrating that even a 132 nm thick Sr_2RuO_4 film on (110) $NdGaO_3$ is commensurately strained.

High-angle annular dark-field scanning transmission electron microscopy (HAADF-STEM) was performed on an aberration-corrected FEI Titan Themis operating at 300 keV with a probe convergence semi-angle of 21.4 mrad and inner and outer collection angles of 68 and 340 mrad, respectively. Cross-sectional STEM specimens were prepared with the standard focused ion beam (FIB) lift-out process using an Omniprobe AutoProbe 200 nanomanipulator on an FEI Strata 400 FIB. Atomic resolution STEM images (Fig. 3) of the same 55 nm thick superconducting Sr_2RuO_4 film, characterized in Fig. 2, reveal relatively few structural defects within the field of view (~73 nm). The observed epitaxial orientation relationship is (001) Sr_2RuO_4 ∥ (110) $NdGaO_3$ and [100] Sr_2RuO_4 ∥ [001] $NdGaO_3$, consistent with prior work.[36] The spacing between out-of-phase boundaries propagating through the thickness of the film is greater than the in-plane coherence length ($\xi_{ab}(0)$) of ~66 nm measured on Sr_2RuO_4 single crystals[11] indicating that the growth temperature is high enough to minimize the incorporation of these defects that can destroy superconductivity. There are some regions [Fig. 3(b)] especially near the substrate-film interface where the local stoichiometry corresponds to that of $Sr_3Ru_2O_7$, which is likely due to the narrow growth window for Sr_2RuO_4. Such structural variation was observed in several superconducting films. Note that inclusions of $Sr_3Ru_2O_7$ and $SrRuO_3$ are also seen in single crystals of Sr_2RuO_4 grown slightly outside the optimal conditions.[37] The presence of these impurity phases in Sr_2RuO_4 single crystals leads to a suppression of the measured T_c.[37] An atomic force microscope (AFM) image of the same 55 nm thick Sr_2RuO_4 film is shown in Fig. 4. The RMS roughness is ~7.2 Å.
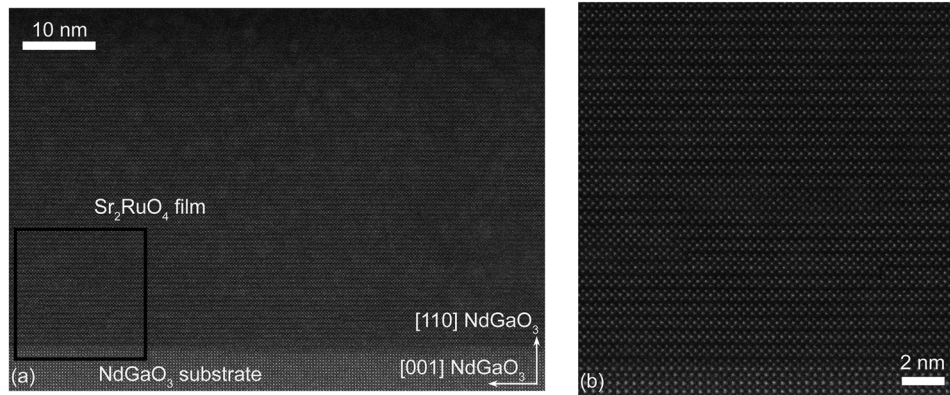
FIG. 3. (a) HAADF-STEM image of the same 55 nm thick Sr_2RuO_4 film grown on a (110) $NdGaO_3$ substrate characterized in Fig. 2 showing a region of the film with representative structural quality. No out-of-phase boundaries propagate through the thickness of the film within the field of view (~73 nm). The arrows indicate the in-plane and out-of-plane crystallographic axes of the substrate. (b) Higher magnification HAADF-STEM image of the region marked by the black box in (a) shows a sharp substrate-film interface and a few layers where the local stoichiometry corresponds to that of $Sr_3Ru_2O_7$. This is not surprising considering the narrowness of the growth window for Sr_2RuO_4 indicated in Fig. 1.

Resistivity as a function of temperature for more than 80 Sr_2RuO_4 films grown on (110) $NdGaO_3$ was measured in a four-point rectangular geometry from room temperature to 4 K to screen out films that do not have a sufficiently high in-plane residual resistivity ratio (RRR) [$\rho_{ab}(300 \text{ K})/\rho_{ab}(4 \text{ K})$]. Films deemed phase pure by XRD, grown in the SrO(s) + RuO_x(g) region of the TOMBE diagram, consistently have $\rho_{ab}(4 \text{ K}) > 5 \ \mu\Omega \cdot \text{cm}$ and do not superconduct above 0.4 K. Only films with $\rho_{ab}(4 \text{ K}) < 4 \ \mu\Omega \cdot \text{cm}$, corresponding to RRRs > 30–33, were observed to undergo a superconducting transition above 0.4 K, the measurement limit of our low-temperature setup described below. This is similar to the case of growth outside the stability window for epitaxial yttrium barium copper oxide thin films (with nominal composition $YBa_2Cu_3O_7$),[38] which are non-superconducting when grown outside of the thermodynamic stability window.[39] Resistivity as a function of temperature for the same sample characterized by XRD, STEM, and AFM (Figs. 2–4, respectively) is shown in Fig. 5(a), indicating a RRR of 69.

The superconducting transition was measured in a Quantum Design Physical Property Measurement System (PPMS) equipped with a ^{3}He insert to measure electrical transport as a function of temperature from 300 K down to 0.4 K. Electrical contacts were made by wire bonding aluminum
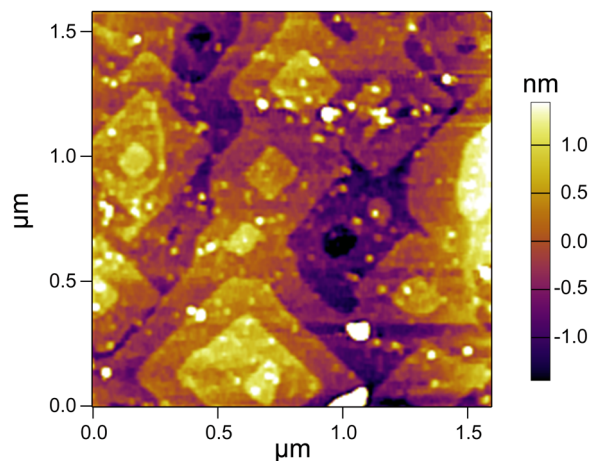
FIG. 4. AFM image of the same 55 nm thick Sr_2RuO_4 film grown on a (110) $NdGaO_3$ substrate showing an islanded growth mode. The RMS roughness is ~7.2 Å.
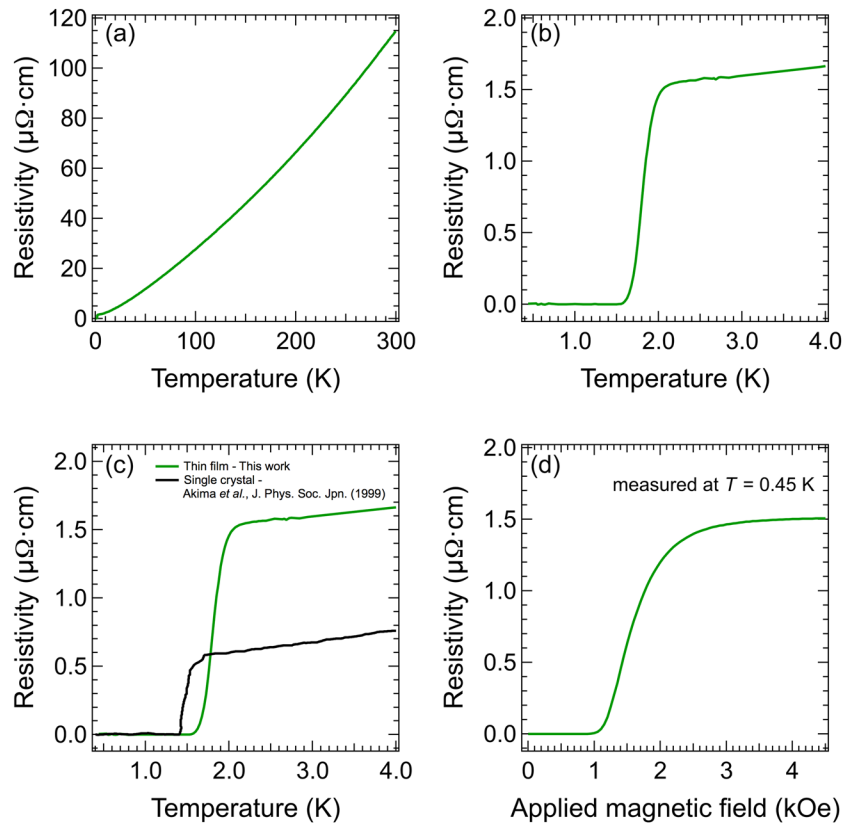
FIG. 5. (a) Resistivity as a function of temperature of the same 55 nm thick Sr_2RuO_4 film grown on the (110) $NdGaO_3$ substrate. The in-plane residual resistivity ratio (RRR) [ρ_{ab}(300 K)/ρ_{ab}(4 K)] of this Sr_2RuO_4 film is 69. (b) A closeup plot of the superconducting transition showing a T_c of 1.8 K. (c) Comparison of the superconducting transition of our Sr_2RuO_4 thin film with a Sr_2RuO_4 single crystal illustrating the relative broad transition in our film. (d) Magnetoresistance at a fixed temperature of 0.45 K shows the suppression of superconductivity as a function of a magnetic field applied along the [001] direction of the film.

wires from gold pads on the PPMS sample holder directly to the surface of the 5 mm × 10 mm film in a four-point linear geometry. Each of the wire bonds was spaced apart by ∼2 mm along the longer dimension of the sample. Note that the film was not patterned, so the current is not constrained in how it flows. The superconducting transition for the same film characterized in Figs. 2 and 3 is shown in Fig. 5(b), measured at zero magnetic field with an excitation current of $I = 100$ μA. The T_c is 1.8 K. The full width of the superconducting transition in temperature ($\Delta T \sim 0.4$ K) is relatively broad compared to single crystals ($\Delta T < 0.1$ K), as shown in Fig. 5(c). This is likely due to the presence of percolative superconducting pathways, which have a higher T_c than the majority of the film. The residual resistivity of the highest-quality Sr_2RuO_4 superconducting film, we have grown to date, is ∼1.5 $\mu\Omega$·cm, which is relatively high when compared to ∼100 nΩ·cm for the highest purity Sr_2RuO_4 single crystals.[13] This suggests that with further reduction in impurities and planar defects in our films, it might be possible to attain an even higher T_c and a sharper superconducting transition. Figure 5(d) shows the magnetoresistance of the same film measured at 0.45 K with the magnetic field applied along the [001] direction of the film. A tangent-line construction gives an upper critical field of $H_{c2\parallel c}$(0.45 K) = 2.0 kOe. The suppression of the zero resistance state with an applied magnetic field confirms that the resistive transition measured here [Fig. 5(b)] is indeed the result of superconductivity.

As is evident from Fig. 5(c), the onset of superconductivity of our Sr_2RuO_4 films grown on (110) $NdGaO_3$ is higher than that for Sr_2RuO_4 single crystals and higher than any other reports for Sr_2RuO_4 thin films. Note that all prior reports of superconducting Sr_2RuO_4 films involved growth on (100) $(LaAlO_3)_{0.29}$—$(SrAl_{1/2}Ta_{1/2}O_3)_{0.71}$ (LSAT) substrates.[24–26] The misfit strain, at room temperature,

of the Sr_2RuO_4 film on (110) $NdGaO_3$ reported here is -0.39% along the [001] in-plane direction of the substrate and -0.16% along the [1$\bar{1}$0] direction of the substrate. The anisotropic in-plane misfit strain in the Sr_2RuO_4 film grown on the (110) $NdGaO_3$ substrate could be the cause for the enhancement in onset T_c. This is consistent with recent studies showing that the T_c of Sr_2RuO_4 single crystals is highly sensitive to uniaxial strain.[14,15] To test this hypothesis more carefully, future work on epitaxial thin films should focus on quantitatively disentangling factors that enhance T_c (e.g., lattice strain) from those that suppress T_c (e.g., defects) following the pioneering work on single crystals.[12,14,15]

In summary, we have outlined and demonstrated an adsorption-controlled growth window for Sr_2RuO_4 thin films using molecular-beam epitaxy. We provide an explanation based on thermodynamic calculations for the origin of the narrow growth window for achieving superconducting thin films. We hope that this work clarifies some of the mysteries surrounding the growth of superconducting Sr_2RuO_4 thin films. Finally, growth within this window has yielded superconducting Sr_2RuO_4 thin films with a T_c of up to 1.8 K on (110) $NdGaO_3$ substrates, the highest reported to date for Sr_2RuO_4 thin films.

See supplementary material for additional TOMBE diagrams illustrating the expanded growth window for Sr_2RuO_4 attained by tuning the excess ruthenium flux.

[1] T. M. Rice and M. Sigrist, J. Phys.: Condens. Matter **7**, L643 (1995).
[2] G. M. Luke, Y. Fudamoto, K. M. Kojima, M. I. Larkin, J. Merrin, B. Nachumi, Y. J. Uemura, Y. Maeno, Z. Q. Mao, Y. Mori, H. Nakamura, and M. Sigrist, Nature **394**, 558 (1998).
[3] K. Ishida, H. Mukuda, Y. Kitaoka, K. Asayama, Z. Q. Mao, Y. Mori, and Y. Maeno, Nature **396**, 658 (1998).
[4] A. P. Mackenzie and Y. Maeno, Physica B **280**, 148 (2000).
[5] A. P. Mackenzie and Y. Maeno, Rev. Mod. Phys. **75**, 657 (2003).
[6] K. Deguchi, Z. Q. Mao, and Y. Maeno, J. Phys. Soc. Jpn. **73**, 1313 (2004).
[7] Y. Maeno, S. Kittaka, T. Nomura, S. Yonezawa, and K. Ishida, J. Phys. Soc. Jpn. **81**, 011009 (2012).
[8] C. Kallin, Rep. Prog. Phys. **75**, 042501 (2012).
[9] A. P. Mackenzie, T. Scaffidi, C. W. Hicks, and Y. Maeno, npj Quantum Mater. **2**, 40 (2017).
[10] Y. Maeno, H. Hashimoto, K. Yoshida, S. Nishizaki, T. Fujita, J. G. Bednorz, and F. Lichtenberg, Nature **372**, 532 (1994).
[11] T. Akima, S. Nishizaki, and Y. Maeno, J. Phys. Soc. Jpn. **68**, 694 (1999).
[12] A. P. Mackenzie, R. K. W. Haselwimmer, A. W. Tyler, G. G. Lonzarich, Y. Mori, S. Nishizaki, and Y. Maeno, Phys. Rev. Lett. **80**, 161 (1998).
[13] M. E. Barber, A. S. Gibbs, Y. Maeno, A. P. Mackenzie, and C. W. Hicks, Phys. Rev. Lett. **120**, 076602 (2018).
[14] C. W. Hicks, D. O. Brodsky, E. A. Yelland, A. S. Gibbs, J. A. N. Bruin, M. E. Barber, S. D. Edkins, K. Nishimura, S. Yonezawa, Y. Maeno, and A. P. Mackenzie, Science **344**, 283 (2014).
[15] A. Steppke, L. Zhao, M. E. Barber, T. Scaffidi, F. Jerzembeck, H. Rosner, A. S. Gibbs, Y. Maeno, S. H. Simon, A. P. Mackenzie, and C. W. Hicks, Science **355**, eaaf9398 (2017).
[16] B. Burganov, C. Adamo, A. Mulder, M. Uchida, P. D. C. King, J. W. Harter, D. E. Shai, A. S. Gibbs, A. P. Mackenzie, R. Uecker, M. Bruetzam, M. R. Beasley, C. J. Fennie, D. G. Schlom, and K. M. Shen, Phys. Rev. Lett. **116**, 197003 (2016).
[17] Z. Q. Mao, Y. Mori, and Y. Maeno, Phys. Rev. B **60**, 610 (1999).

[18] Y.-T. Hsu, W. Cho, A. F. Rebola, B. Burganov, C. Adamo, K. M. Shen, D. G. Schlom, C. J. Fennie, and E.-A. Kim, Phys. Rev. B **94**, 045118 (2016).

[19] P. M. R. Brydon and D. Manske, Phys. Rev. Lett. **103**, 147001 (2009).

[20] P. M. R. Brydon, C. Iniotakis, D. Manske, and M. Sigrist, Phys. Rev. Lett. **104**, 197001 (2010).

[21] P. Gentile, M. Cuoco, A. Romano, C. Noce, D. Manske, and P. M. R. Brydon, Phys. Rev. Lett. **111**, 097003 (2013).

[22] B. van Heck, A. R. Akhmerov, F. Hassler, M. Burrello, and C. W. J. Beenakker, New J. Phys. **14**, 035019 (2012).

[23] T. Hyart, B. van Heck, I. C. Fulga, M. Burrello, A. R. Akhmerov, and C. W. J. Beenakker, Phys. Rev. B **88**, 035121 (2013).

[24] Y. Krockenberger, M. Uchida, K. S. Takahashi, M. Nakamura, M. Kawasaki, and Y. Tokura, Appl. Phys. Lett. **97**, 082502 (2010).

[25] J. Cao, D. Massarotti, M. E. Vickers, A. Kursumovic, A. Di Bernardo, J. W. A. Robinson, F. Tafuri, J. L. MacManus-Driscoll, and M. G. Blamire, Supercond. Sci. Technol. **29**, 095005 (2016).

[26] M. Uchida, M. Ide, H. Watanabe, K. S. Takahashi, Y. Tokura, and M. Kawasaki, APL Mater. **5**, 106108 (2017).

[27] M. A. Zurbuchen, Y. Jia, S. Knapp, A. H. Carim, D. G. Schlom, L.-N. Zou, and Y. Liu, Appl. Phys. Lett. **78**, 2351 (2001).

[28] M. A. Zurbuchen, Y. Jia, S. Knapp, A. H. Carim, D. G. Schlom, and X. Q. Pan, Appl. Phys. Lett. **83**, 3891 (2003).

[29] M. A. Zurbuchen, W. Tian, X. Q. Pan, D. Fong, S. K. Streiffer, M. E. Hawley, J. Lettieri, Y. Jia, G. Asayama, S. J. Fulk, D. J. Comstock, S. Knapp, A. H. Carim, and D. G. Schlom, J. Mater. Res. **22**, 1439 (2007).

[30] H. P. Nair, Y. Liu, J. P. Ruf, N. J. Schreiber, S.-L. Shang, D. J. Baek, B. H. Goodge, L. F. Kourkoutis, Z.-K. Liu, K. M. Shen, and D. G. Schlom, APL Mater. **6**, 046101 (2018).

[31] K. T. Jacob, K. T. Lwin, and Y. Waseda, Mater. Sci. Eng.: B **103**, 152 (2003).

[32] V. Leca, D. H. A. Blank, and G. Rijnders, e-print arXiv:1202.2256 (2012).

[33] L. Walz and F. Lichtenberg, Acta Crystallogr., Sect. C: Cryst. Struct. Commun **49**, 1268 (1993).

[34] M. Schmidbauer, A. Kwasniewski, and J. Schwarzkopf, Acta Crystallogr., Sect. B: Struct. Sci. **68**, 8 (2012).

[35] J. Paglione, C. Lupien, W. A. MacFarlane, J. M. Perz, L. Taillefer, Z. Q. Mao, and Y. Maeno, Phys. Rev. B **65**, 220506 (2002).

[36] S. Madhavan, Y. Liu, D. G. Schlom, A. Dabkowski, H. A. Dabkowska, Y. Suzuki, I. Takeuchi, Z. Trajanovic, and R. P. Sharma, IEEE Trans. Appl. Supercond. **7**, 2063 (1997).

[37] Z. Q. Mao, Y. Maenoab, and H. Fukazawa, Mater. Res. Bull. **35**, 1813 (2000).

[38] R. H. Hammond and R. Bormann, Physica C **162-164**, 703 (1989).

[39] V. Matijasevic, P. Rosenthal, K. Shinohara, A. F. Marshall, R. H. Hammond, and M. R. Beasley, J. Mater. Res. **6**, 682 (1991).
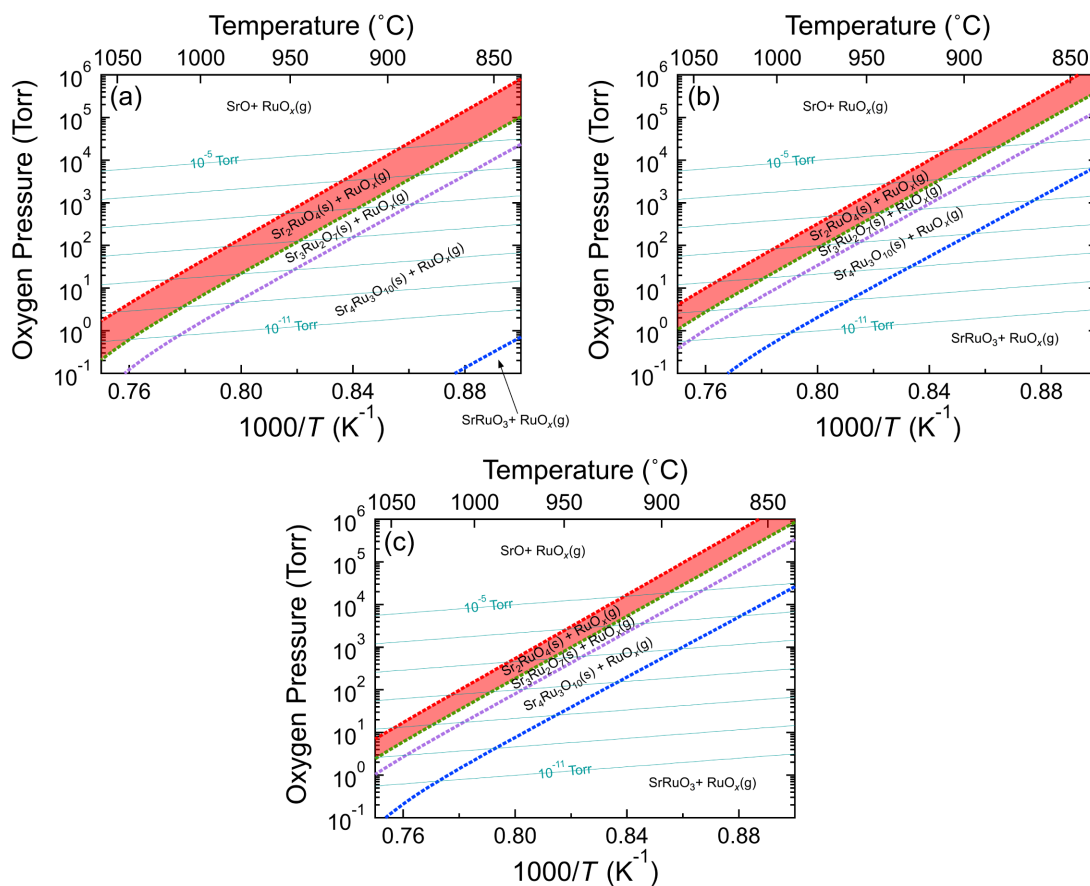
Fig. S1: TOMBE diagram calculated for a fixed incident ruthenium flux of 2.00×10^{13} atoms/cm$^2 \cdot$s and excess ruthenium fluxes of (a) 1.01×10^{13} atoms/cm$^2 \cdot$s, (b) 1.5×10^{13} atoms/cm$^2 \cdot$s, and (c) 1.95×10^{13} atoms/cm$^2 \cdot$s. It is evident that a reduction in the excess ruthenium flux causes the thermodynamic growth window for adsorption controlled growth window for Sr$_2$RuO$_4$ (shaded red) to expand in both growth temperature and oxygen pressure.